Journal of Sports Sciences, April 2007; 25(6): 643 – 650

Routledge
Taylor & Francis Group

A fluid dynamic investigation of the Big Blade and Macon oar blade designs in rowing propulsion

NICHOLAS CAPLAN[1] & TREVOR N. GARDNER[2]

[1]*Health, Exercise and Sports Performance Research Group, Division of Sport Sciences, Northumbria University, Newcastle-upon-Tyne and* [2]*Biomechanics Research Group, School of Sport and Exercise Sciences, University of Birmingham, Birmingham, UK*

(Accepted 24 March 2006)

Abstract
The purpose of this investigation was to examine the fluid dynamic characteristics of the two most commonly used oar blades: the Big Blade and the Macon. Scaled models of each blade, as well as a flat Big Blade, were tested in a water flume using a quasi-static method similar to that used in swimming and kayaking research. Measurement of the normal and tangential blade forces enabled lift and drag forces generated by the oar blades to be calculated over the full range of sweep angles observed during a rowing stroke. Lift and drag force coefficients were then calculated and compared between blades. The results showed that the Big Blade and Macon oar blades exhibited very similar characteristics. Hydraulic blade efficiency was not therefore found to be the reason for claims that the Big Blade could elicit a 2% improvement in performance over the Macon. The Big Blade was also shown to have similar characteristics to the flat plate when the angle of attack was below 90°, despite significant increases in the lift coefficient when the angle of attack increased above 90°. This result suggests that the Big Blade design may not be completely optimized over the whole stroke.

Keywords: *Drag, lift, oar blade, rowing*

Introduction

To enhance performance in rowing, it is important to maintain a high mean boat velocity (Schneider & Hauser, 1981), which requires a highly efficient stroke. This is achieved by the crew applying large input forces to the oar handle that are transferred to the water by the oar shaft and blade as output forces (Figure 1).

The first oars for rowing were constructed from wood (Herberger, 1987), and the oar blades were of a long, flat, and thin ''pencil'' design (Dudhia, 2000). In the 1950s, crews started experimenting with shorter, wider, and curved blades, and in 1958 a German crew used what is now known as the ''Macon'' blade (Figure 2), named after the venue for the World Championships of that year (Pinkerton, 1992; Pomponi, 1994; Sayer, 1996). Blade shape did not change significantly from the Macon shape until 1991 when Concept 2 introduced an asymmetrical blade shape, named the ''Big Blade'' after its larger surface area (Dreher, 1997; Dreissigacker & Dreissigacker, 2005; Nolte, 1993), with this new design being made possible through improved understanding of composite materials (Pinkerton, 1992). As was also the case in boat design, composite materials allowed for lighter blades with increased stiffness, therefore improving the efficiency of the blade (Dal Monte & Komor, 1989; Sayer, 1996). Despite the improvements in the construction of oar blades, their fluid dynamic characteristics have yet to be fully explored, with blade designs being based upon trial-and-error approaches (Pinkerton, 1992).

The sequence of oar blade movements during the stroke that give rise to the propulsion produced by the blade has previously been broken down into four phases (Figure 3). These illustrate the relative magnitudes of propulsive lift and drag forces generated by the oar blade for varying sweep angles (Dreissigacker & Dreissigacker, 2000). The movement of the oar blade relative to the water during these phases will generate both lift and drag forces similar to any aerofoil (Nolte, 1984). Figure 3 shows that for optimal stroke efficiency, high lift forces must be achieved at the start (phases 1 and 2) and end (phase 4) of the stroke, with high drag forces being

Correspondence: N. Caplan, Division of Sport Sciences, Northumbria University, Wynne Jones Centre, Ellison Place, Newcastle-upon-Tyne NE1 8ST, UK. E-mail: nick.caplan@northumbria.ac.uk

ISSN 0264-0414 print/ISSN 1466-447X online © 2007 Taylor & Francis
DOI: 10.1080/02640410600809985

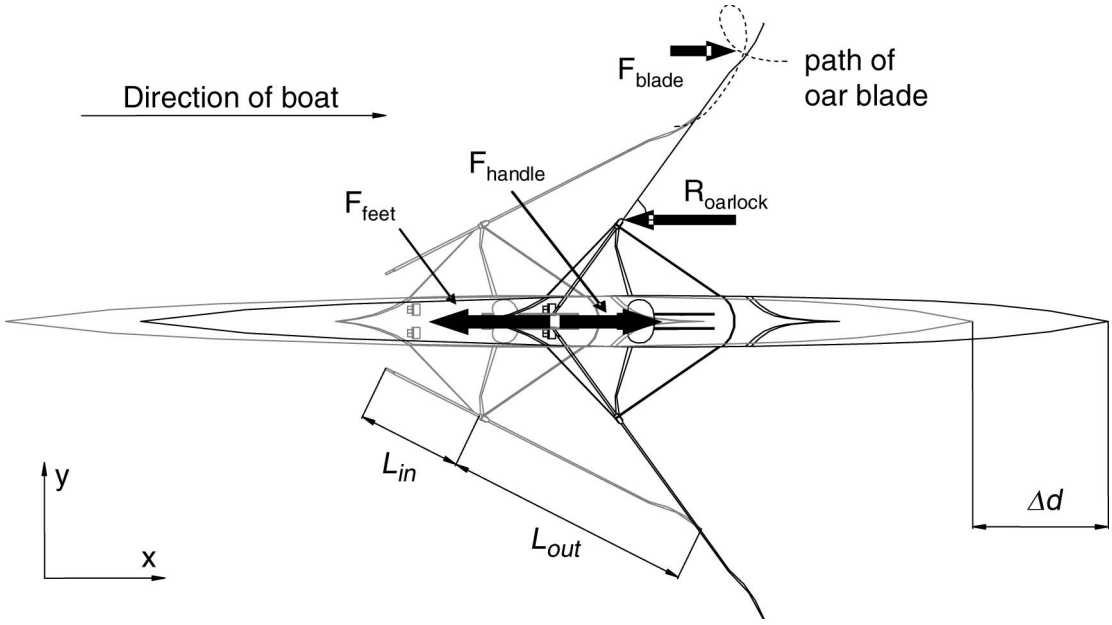

Figure 1. Overhead view of a single scull showing the forces that occur during the drive phase of the stroke, together with the oar shaft dimensions. The single scull is shown at two instants and the measured path of the centre of the oar blade is shown for a right-handed oar (--) (Kleshnev, 1999).

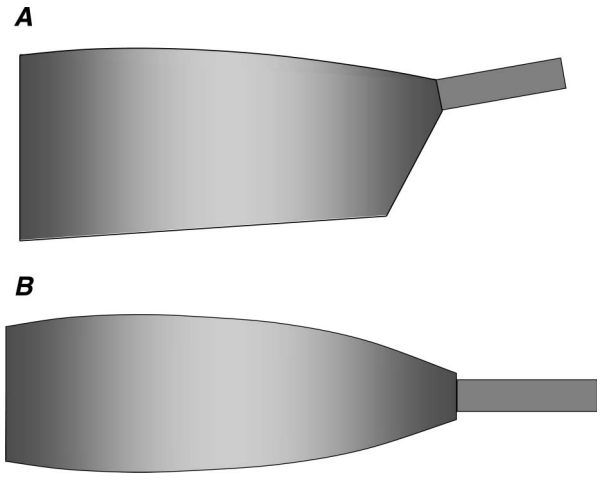

Figure 2. Frontal views of the Big Blade (A) and Macon (B) oar blade designs, together with the orientation of oar shaft attachment for each.

required as the oar shaft approaches a position perpendicular to the line of the boat (phase 3).

Due to the complex sequence of movements between the oar blade and the water affecting lift and drag, the fluid dynamic characteristics of oar blades must be determined to assess the success of any oar blade design. Yet, in spite of the profound effect of hydraulic performance of oar blades on rowing propulsion, few attempts have been made to measure these characteristics (Barre & Kobus, 1998; Jonker & Yenson, 2002; Ramsey, 1993). The studies that have done used a dynamic approach, which limits the applicability of the data to only the blade movement paths produced by their methods. Because of the complex and variable path of the oar blade in rowing, it is more appropriate to use a quasi-static approach (Toussaint, Van den Berg, & Beek, 2002), as used previously in swimming (Berger, de Groot, & Hollander, 1995) and kayaking (Sumner, Sprigings, Bugg, & Heseltine, 2003), which involves either the hand or blade being held static in a water flume at a range of angles similar to those encountered during each stroke, and the resultant fluid force being recorded at each sweep angle. Using this method allows the force characteristics of each oar blade to be applied to any rowing condition, unlike previous dynamics studies (Barre & Kobus, 1998; Jonker & Yenson, 2002; Ramsey, 1993). These force data can then be combined with measured, or modelled, kinematic data to estimate propulsive forces during the stroke. Berger, Hollander and de Groot (1999) recently showed that there was only a 5% difference between using measured propulsive force and quasi-static data, with some of this error being due to the error in simulating hand kinematics, which suggests that quasi-static simulations are appropriate and accurate. A limitation of using the quasi-static approach, however, is that forces generated by the development of any non-steady-state vortices about the oar blade are ignored. However, to take account of these dynamic factors, a complex computational fluid dynamic model would be required, which was beyond the scope of the present study.

The purpose of the present investigation was, therefore, to determine the fluid dynamic characteristics of the Big Blade and Macon oar blade designs

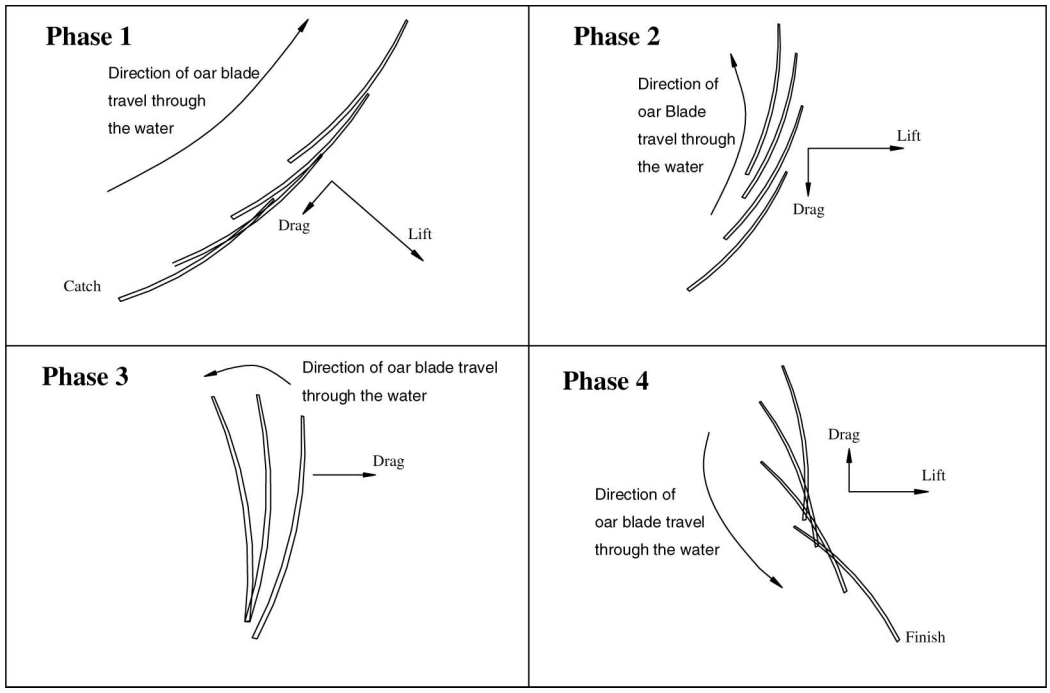

Figure 3. The movement of a right-handed oar blade during the drive phase of the rowing stroke with the boat moving from left to right. The approximate directions of the lift and drag forces generated are indicated (adapted from Dreissigacker & Dreissigacker, 2000).

to assess their ability to successfully generate lift and drag forces during the rowing stroke. It was expected that the Big Blade would show an improved ability to generate fluid forces when compared with the Macon in line with the performance advantage claimed by the manufacturers, and that blade curvature would also have a positive influence on the fluid forces generated.

Methods

Oar blades

The fluid dynamic tests were performed in a water flume that had a free stream width and depth of 0.64 m and 0.15 m, respectively. Due to the inherent edge resistance effects on the free stream velocity, it was decided that quarter scale oar blade models should be used so that the length of the blades was less than a quarter of the flume width and remained in the part of the flume where velocity reductions were minimal. The model blades were fabricated from 1.80-mm thick aluminium sheet, which was shown by dimensional analysis to provide sufficient stiffness to be able to discount any influence of oar blade bending. Although this model thickness transfers to a blade thickness of 7.2 mm, compared with the full size oar blade thickness of 5 mm, a model thickness of 1.8 mm was required to avoid any influence of blade flexing. Compared with the influence of the shape of the blade, this increase in blade thickness is unlikely to have a significant influence on blade characteristics. Several oar blade designs were tested, including the Macon and Big Blade designs (Concept 2, Morrisville, USA), and a flat plate with the same shape and projected area as the Big Blade. Both the Big Blade and Macon oar blade designs have both longitudinal and lateral curvature. However, due to manufacturing limitations, only the longitudinal curvature could be modelled. Traditionally, both oar blade designs have a spine that runs along the line of the oar shaft and extends approximately half way along the length of the blade. However, recent advances in oar blade design have seen the removal of this spine from the face of the blade (e.g. Big Blade Smoothie, Concept 2, Morrisville, USA). Therefore, the model blades used in the present investigation were manufactured without a spine. The flat plate was tested to help determine the influence of blade curvature.

Experimental set-up

To measure the forces being applied to the oar blade models, a measurement system was designed such that the model blades could be held static in the flume at a range of angles relative to the direction of free stream. The blades were attached to a model oar shaft, with their normal orientations relative to the shaft (Figure 2), and the model shaft made an angle of 10° with the water surface. This model oar shaft was attached to a vertical bar, and strain gauges

located on both the oar shaft and vertical bar recorded the normal and tangential fluid forces generated by the model oar blades (Figure 4).

This allowed for the determination of lift and drag forces using the equations,

$$F_{\text{Lift}} = F_{\text{T}} \sin\alpha + F_{\text{N}} \cos\alpha \quad (1)$$

and

$$F_{\text{Drag}} = F_{\text{N}} \sin\alpha - F_{\text{T}} \cos\alpha \quad (2)$$

where F_{T} is the blade force acting tangentially to the blade chord line (Figure 5), F_{N} is the blade force acting normally to the blade chord line, and α is the angle of attack between the blade chord line and the free stream direction of fluid flow (Figure 5). The angular position of the vertical bar in the horizontal plane, and hence the angle α of the oar shaft, was measured using a 360° smart position sensor (601-1045, Vishay Spectrol, UK), which had a stated linearity of ±1% and a resolution of 0.5°. This position sensor was powered by a fixed voltage power supply (5 V), and the output of the position sensor was displayed on a digital volt meter. For a detailed description of the design and calibration of the measurement system, and the reduction of lift and drag forces from the strain gauge recordings, see Caplan and Gardner (2005).

Lift force, F_{L}, and drag force, F_{D}, of an oar blade can be modelled by the relationships,

$$F_{\text{L}} = \frac{1}{2} C_{\text{L}} \rho A V^2 \quad (3)$$

and

$$F_{\text{D}} = \frac{1}{2} C_{\text{D}} \rho A V^2 \quad (4)$$

where ρ is the fluid density, A is the projected area of the oar blade measured perpendicularly to the face of the blade, and V is the relative velocity between the oar blade and water (Munson, Young, & Okiishi, 2002). C_{L} and C_{D} are dimensionless force coefficients that are dependent upon the oar blade shape and the angle of attack between oar blade chord line and fluid flow direction. To compare the fluid dynamic characteristics of oar blade designs, it is appropriate to calculate and compare the force coefficients to discount any influence of fluid velocity, fluid density, and projected area.

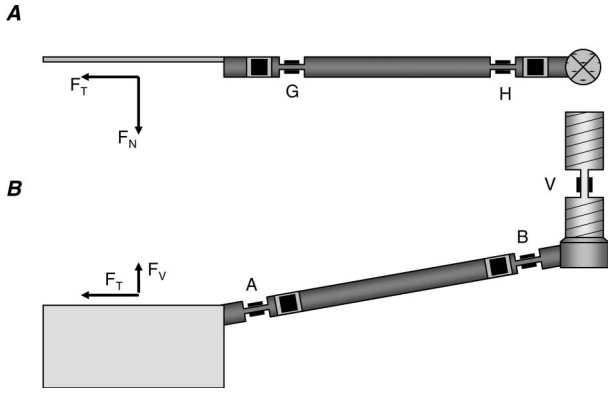

Figure 4. Plan (A) and side (B) views of the system used to measure the normal and tangential oar blade forces, through the use of strain gauges A, B, G, H, and V.

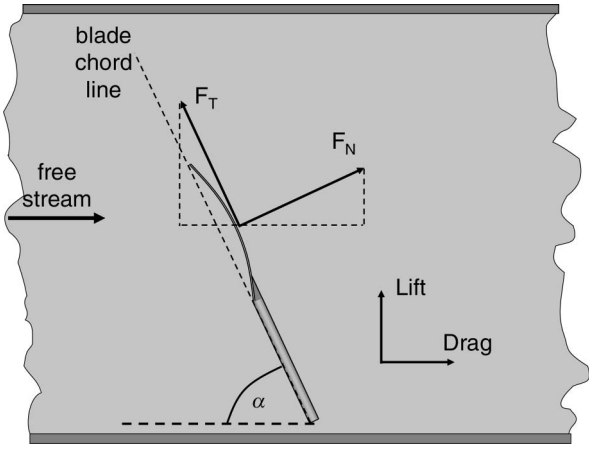

Figure 5. Plan view of the water flume showing the orientation of the oar blade. The directions of lift and drag forces are illustrated, together with the measured normal and tangential oar blade forces and the chord line of the blade.

Experimental protocol

Before each blade was tested, reference flow conditions were established by making a point velocity measurement at a depth of 25 mm from the water surface in the centre of the flume using a miniature current flow meter probe (403, Nixon, UK), and the rotational frequency of the probe was displayed on a flow meter (Streamflo 400, Nixon, UK).

A 10-s baseline force measurement was taken and the data averaged over the duration of this period. The oar blade was then placed in the flume so that the blade chord line was in line with the direction of free stream ($\alpha = 0°$), and with the top edge of the blade flush with the water surface. Signals from the strain gauges passed through a custom-made strain gauge amplifier before passing to an analog-to-digital card (PC-DAS 16/12, Measurement Computing, USA), which sampled the data at a frequency of 2.5 kHz for a period of 15 s for each trial. Four 15-s trials were collected at each angle of attack.

The angle of attack was increased in 5° intervals between 0 and 180°. The data collected during each 15-s collection period were averaged to provide four mean voltages for each strain gauge bridge at each angle. These voltages allowed for the calculation of lift and drag forces as described

earlier and in Caplan and Gardner (2005). The water temperature was 16°, which equated to a fluid density of 999 kg · m^{-3}. This value, together with the projected areas of the oar blades given in Table I, the measured fluid velocity, and lift and drag forces were substituted into equations (1) and (2) to provide lift and drag coefficients for each angle of attack tested. A macro image analyser (Carl Zeiss, Germany) was used to photograph the blades from directly above, and the software Axio Vision (Carl Zeiss, Germany) was subsequently used to determine the projected area of each blade image shown in Table I.

Influence of Reynolds number

As with any fluid dynamic test involving the use of scaled models, both geometric (aspect ratio) and dynamic (Reynolds number) similarity must be achieved for the model data to be directly applied to the real-life situations. As the models were scaled exactly from the full-size oar blades, geometric similarity was met. However, because of the scale of the models and the maximum velocity that could be achieved by the water flume, it was not possible to achieve Reynolds number similarity. It was therefore necessary to determine the Reynolds number dependence of the lift and drag coefficients. Reynolds number is given by

$$\mathrm{Re} = \frac{\rho V l}{\mu} \tag{5}$$

where ρ is the fluid density, V is the fluid velocity, l is a characteristic length of the object, and μ is the kinematic viscosity of the fluid (Munson *et al.*, 2002). The dependence of the model data on Reynolds number can therefore be determined by varying either the model size or relative free stream velocity. Due to the edge effects of the water flume, with the fluid velocity reducing as the edges are approached, the measured force coefficients would be influenced by a reduced average free stream velocity across the frontal area of the blade if the blade size was increased. Therefore, the flat plate, the simplest of blade designs, was tested at a range of fluid velocities, (0.4 – 0.85 m · s^{-1}) using the protocol described above. It was found that lift and drag coefficients were independent of Reynolds number with a free stream velocity above 0.7 m · s^{-1}, as discussed in the next section. A fluid velocity of 0.75 m · s^{-1} was therefore used for the remainder of the tests, which was high enough to overcome any influence of Reynolds number, but not so high that the increasing turbulence of the water interfered with the measurement system.

Table I. Projected areas for the model oar blades tested.

Blade	Projected area (cm^2)
Flat plate	77.42
Big Blade	77.41
Macon	67.48

Data analysis

The calculated lift and drag coefficients were compared between oar blade designs. Independent samples *t*-tests were used at each angle, α, to determine if the difference between oar blade designs was significant at each angle tested, with a 99% confidence level ($P < 0.01$) being used throughout.

Results and discussion

The simplest of oar blade designs was the flat plate with the same perimeter shape and projected area as the Big Blade. Figure 6 shows both drag and lift coefficients for this oar blade plotted against angle of attack. An angle of attack of less than 90° indicated that the leading edge of the oar blade was the tip of the blade, and an angle of attack greater than 90° indicated that the leading edge had changed to the shaft end of the oar blade.

The drag coefficient was seen to increase with angle of attack until an angle close to 90° was reached, at which point the maximum (C_{Dmax}) was approximately 2. As the angle of attack increased further, the drag coefficient reduced towards zero.

The lift coefficient increased with angle of attack until a maximum (C_{Lmax}) was reached at approximately 40 – 45°, and reduced to zero at 90°. As the angle of attack continued to increase, with the leading edge having changed to the shaft end of the blade, the lift coefficient decreased to a minimum (C_{Lmin}) at approximately 135°. As the angle of attack increased further, the lift coefficient increased to

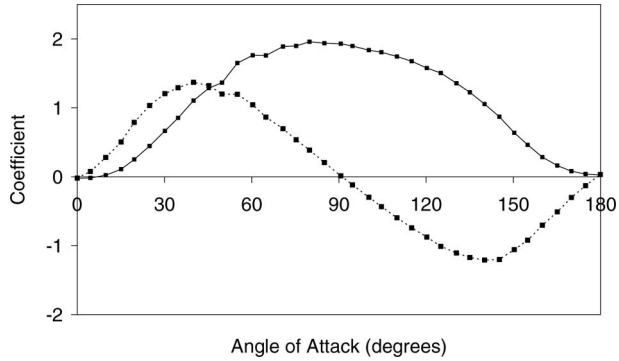

Figure 6. Lift (- - -) and drag (—) coefficients are plotted against angle of attack for a flat plate.

zero. Although the lift coefficient was negative at angles of attack greater than 90°, the negative sign simply indicated that the direction of the lift force generated by the oar blade changed direction by 180°.

To determine the influence of Reynolds number on the measured data, C_{Dmax}, C_{Lmax}, and C_{Lmin} were compared for the flat plate presented in Figure 6 at a range of free stream velocities. Figure 7 shows that both C_{Lmax} and C_{Lmin} were virtually unaffected by velocity, and that the drag coefficient is independent of velocity above 0.7 m · s^{-1}.

The data presented in Figure 7 agreed well with previously published data for the forearm in swimming (Berger *et al.*, 1995; Bixler & Riewald, 2002). Berger *et al.* (1995) showed that, for a prosthetic human forearm and hand that was dragged through a towing tank, the lift and drag coefficients were only slightly dependent on velocity at free stream velocities above 0.7 m · s^{-1}, where the Reynolds number at this velocity was 6.29×10^4. Bixler and Riewald (2002) used a computational fluid dynamic model to predict the flow about a similar hand and forearm model and it was predicted that the coefficients were independent of velocity above 1 m · s^{-1}, where the Reynolds number equalled 9.96×10^4. For the flat plate tested here, the Reynolds number at 0.7 m · s^{-1} was 9.44×10^4, which was within previously published ranges for Reynolds number independence, as discussed above.

Figure 8 shows the effect of adding longitudinal curvature to the Big Blade design. It was expected that curvature would increase the magnitude of fluid circulation about the blade, thus increasing lift (Batchelor, 2000). At angles of attack below 90°, however, the lift coefficient is similar for both the flat and curved blades. This result suggests that some mechanism must play a part in the changes in the lift coefficient seen with curvature, which negates the increase in lift expected through added circulation. Although increasing the curvature of the blade should, theoretically, increase the fluid circulation around the blade and therefore increase lift, fluid will also separate away from the back of the blade more easily, increasing the turbulence in the boundary layer of the blade, thus reducing lift and increasing drag. For maximum lift, the boundary layer flow should be laminar and not turbulent. Hoerner and Borst (1985) showed that for low aspect ratio wings, such as the oar blades investigated here, where the aspect ratio (width/height, where height is the longitudinal length relative to free stream direction in this case) is less than 3, the lateral edges, or upper and lower edges for oar blades, play a significant role in the generation of lift. Higher aspect ratio wings simply have a linear increase in lift coefficient with increases in angle of attack (linear lift component), and will typically stall, or reduce its ability to generate lift force, at an angle of attack between 10° and 15°. This linear component of lift is generated by the longitudinal circulation of the boundary layer fluid particles about the blade. Low aspect ratio wings, however, have both a linear and non-linear component of lift. This non-linear component is thought to be due to the fluid flowing around the lateral edges of the wing (upper and lower edges of the oar blade), generating vortices along these edges that act to assist the attachment of the boundary layer to the back of the wing. This increases the stall angle of attack to approximately 45° (Hoerner & Borst, 1985). It is therefore important for the magnitude of these lateral edge vortices to be as great as possible to reduce the separation causing this turbulent flow.

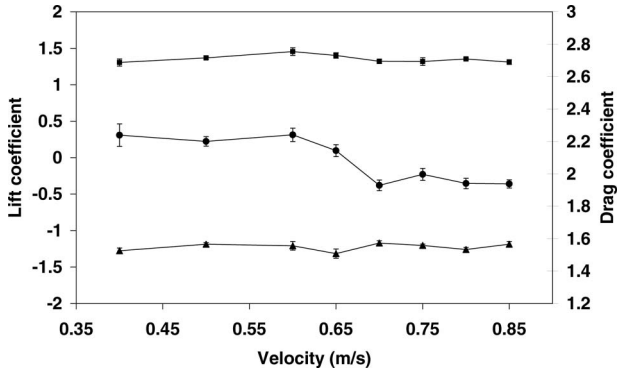

Figure 7. Lift coefficients are shown for both C_{Lmax} (at 45°; ■) and C_{Lmin} (at 135°; ▲), together with drag coefficients for C_{Dmax} (at 90°; ●), at a range of fluid velocities to determine the influence of the Reynolds number.

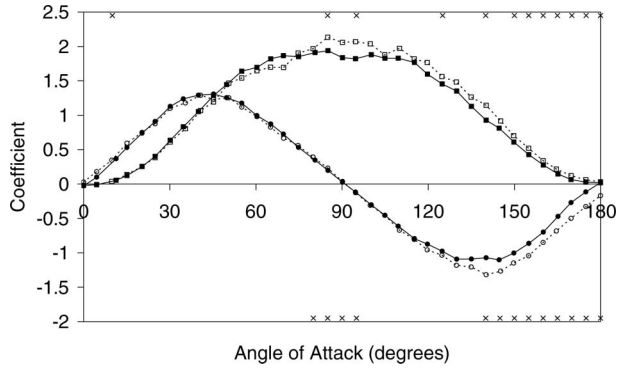

Figure 8. Lift (●/○) and drag (■/□) coefficients are compared for the flat (—) and curved Big Blade (- - -). The × symbols at the top of the figure signify significant differences between blade designs for the drag coefficient and those along the bottom of the figure for the lift coefficient ($P < 0.01$).

Figure 8 shows that the curved Big Blade is able to generate lift more effectively than the flat blade when the shaft end of the blade is acting as the leading edge, with the angle of attack being greater than 90°. For the Big Blade, at these angles of attack, the blade begins to resemble the shape of a delta wing, where the distance between the two edges at any point along its longitudinal axis increases from the leading to the trailing edge. This will result in stronger vortices developing along the upper and lower edges (Hoerner & Borst, 1985), allowing the fluid flow to remain attached to the back of the blade for a longer distance along the blade, resulting in the significant increase in the lift coefficient that is observed between 140° and 180°. The effect of blade curvature on boat propulsion is therefore positive at these angles of attack. At angles of attack below 90°, however, lift is not generated as effectively due to the shape of the upper and lower edges.

The drag coefficient was seen to be greater for the curved blade above 85°. This increase as the angle of attack approaches 180° is due to the increased contribution of form drag as a result of the curvature increasing the area of the blade visible to the oncoming fluid at these low and high angles. At approximately 90°, more fluid is trapped on the face of the blade (Bird, 1975), generating increased drag and hence increasing the drag coefficient. The effect of blade curvature on boat propulsion is therefore positive at angles of attack above 90° and negative at angles below 90°.

Since the introduction of the Big Blade in 1991, performances have improved, suggesting an increase in propulsive efficiency between the Big Blade and the Macon blade designs (Dreissigacker & Dreissigacker, 2000; Pomponi, 1994). However, only small differences in the lift coefficient were observed between the two blades (Figure 9). The lift coefficient was slightly increased for the Big Blade at most angles of attack, although this increase was only significant at a small number of angles when the magnitude of the lift coefficient was small. According to low aspect ratio wing theory, as aspect ratio increases, C_{Lmax} increases and the angle of attack at which C_{Lmax} occurs decreases. At angles of less than 90° this was seen to occur, with the Big Blade (larger aspect ratio) reaching a higher C_{Lmax} at a slightly reduced angle of attack. This effect is less clear at angles greater than 90°.

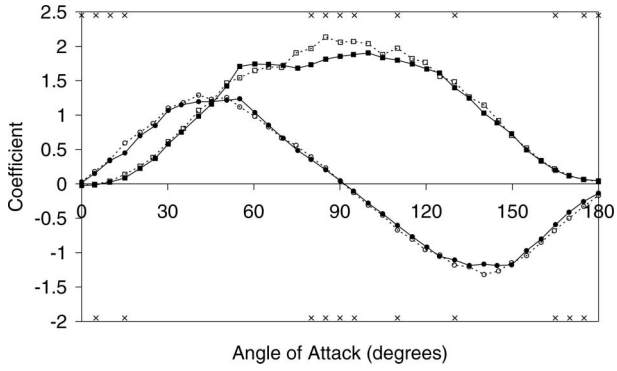

Figure 9. Lift (●/○) and drag (■/□) coefficients are compared for the Big Blade (- - -) and Macon (—) oar blade designs. The × symbols at the top of the figure signify significant differences between blade designs for the drag coefficient and those along the bottom of the figure for the lift coefficient ($P < 0.01$).

The drag coefficient is similar between blades at angles of attack up to 50° and above 145°. However, between 55° and 75°, a small decrease in the drag coefficient is observed for the Macon, but a more substantial increase in this coefficient occurs between 75° and 100° that makes an added positive contribution to propulsion and may contribute to the increased performance claimed for the Big Blade. This effect is likely to be due to the type of fluid flow separation that occurs around the stall point for this blade.

Nolte (1993) suggested that the cause of the supposed improvements in propulsive efficiency with the Big Blade were due to the fluid flow across the face of the blade being less disturbed than with the Macon, due to the upper surface of the Big Blade running parallel to the water surface, generating more lift. The current results suggest this hypothesis to be incorrect, and the lack of substantial difference in blade performances may suggest that the two blades perform similarly. However, the Macon blade has a smaller projected area than the Big Blade, and if rowers used Big Blades and Macon blades of the same projected area, there could be little difference in performance.

In conclusion, the results of this study indicate that the Macon and Big Blade designs have similar fluid dynamic properties at most of the angles studied. However, the Big Blade generated significantly greater drag coefficients at angles of attack around 90°.

It was anticipated that the curved Big Blade would be able to generate significantly greater lift coefficients than the flat plate. The results of the study, however, indicated that this was only true when the angle of attack was greater than 90°, when the leading edge changed from being at the tip to the shaft end of the oar blade. This finding was attributed to the shape of the upper and lower edges of the oar blade, causing it to act in a similar way to a delta wing during the second half of the stroke.

The findings of this study would suggest that current oar blade designs are not completely optimized. It should therefore be possible to transfer propulsive force to the water more efficiently throughout the duration of the stroke.

References

Barre, S., & Kobus, J.-M. (1998). New facilities for measurement and modelling of hydrodynamic loads on oar blades. In S. J. Haake (Ed.), *The engineering of sport* (pp. 251–260). Oxford: Blackwell Science.

Batchelor, G. K. (2000). *An introduction to fluid dynamics.* Cambridge: Cambridge University Press.

Berger, M. A., de Groot, G., & Hollander, A. P. (1995). Hydrodynamic drag and lift forces on human hand/arm models. *Journal of Biomechanics*, *28*, 125–133.

Berger, M. A., Hollander, A. P., & de Groot, G. (1999). Determining propulsive force in front crawl swimming: A comparison of two methods. *Journal of Sports Sciences*, *17*, 97–105.

Bird, W. J. (1975). The mechanics of sculling. *Chartered Mechanical Engineer*, *22*, 91–94.

Bixler, B., & Riewald, S. (2002). Analysis of a swimmer's hand and arm in steady flow conditions using computational fluid dynamics. *Journal of Biomechanics*, *35*, 713–717.

Caplan, N., & Gardner, T. N. (2005). A new measurement system for the determination of oar blade forces in rowing. In M. H. Hamza (Ed.), *Proceedings of the XXth IASTED International Symposium on Biomechanics* (pp. 32–37). Calgary: ACTA Press.

Dal Monte, A., & Komor, A. (1989). Rowing and skulling mechanics. In C. L. Vaughan (Ed.), *Biomechanics of sport* (pp. 53–120). Boca Raton, FL: CRC Press.

Dreher, J. (1997). *Technology discussion: New blade shapes – part 1* (accessed on 8 February 2003 at: www.durhamboat.com/blade.htm).

Dreissigacker, D., & Dreissigacker, P. (2000). Oars – Theory and testing. *Proceedings of the XXIX FISA Coaches Conference* (accessed on 27 May 2005 at: http://www.oarsport.co.uk/oars/c2_vortex_development.php).

Dreissigacker, D., & Dreissigacker, P. (2005). *Dreissigacker oars* (accessed on 8 February 2005 at: http://www.concept2.com/05/oars/oars_home.asp).

Dudhia, A. (2000). A history of Oxford College rowing (accessed on 4 January 2005 at: http://www.atm.ox.ac.uk/rowing/history.html).

Herberger, E. (1987). *Rowing: The GDR textbook of oarsmanship.* Toronto, ONT: Sport Books Publisher.

Hoerner, S. F., & Borst, H. V. (1985). *Fluid-dynamic lift* (2nd edn.). Albuquerque, NM: Hoerner Fluid Dynamics.

Jonker, K., & Yenson, S. (2002). *Quantitative testing of blade performance.* BSc thesis, Massachusetts Institute of Technolgy.

Kleshnev, V. (2001). Propulsive efficiency of rowing. In R. H. Sanders & N. R. Gibson (Eds.), *Proceedings of the XVII International Symposium on Biomechanics in Sports.* Perth: ECU.

Munson, B. R., Young, D. F., & Okiishi, T. H. (2002). *Fundamentals of fluid mechanics* (4th edn.). New York: Wiley.

Nolte, V. (1984). *Die Effektivität des Ruderschlages.* Berlin: Bartels & Wernitz.

Nolte, V. (1993). Do you need hatchets to chop your water? *American Rowing*, July/August, pp. 23–26.

Pinkerton, P. (1992). The Big Blade goes big time. *Australian Rowing*, September, pp. 10–11.

Pomponi, R. (1994). Innovations in oar technology: Transition to a new dominant design (accessed on 1 January 2005 at: http://groups.google.com/groups?hl=en&lr=&ie=UTF-8&selm=renata-2012941115460001%40ctpid-mac-13.mit.edu).

Ramsey, W. D. (1993). *Lift and drag characteristics of rotating oar blades.* BSc thesis, Massachusetts Institute of Technology.

Sayer, B. (1996). *Rowing and sculling: The complete manual.* Bury St Edmunds, UK: St Edmundsbury Press.

Schneider, E., & Hauser, M. (1981). Biomechanical analysis of performance in rowing. In A. Morecki, K. Fidelus, K. Kedzior, & A. Wit (Eds.), *Biomechanics VII-B* (pp. 430–435). Baltimore, MD: University Park Press.

Sumner, D., Sprigings, E. J., Bugg, J. D., & Heseltine, J. L. (2003). Fluid forces on kayak paddle blades of different design. *Sports Engineering*, *6*, 11–20.

Toussaint, H. M., Van den Berg, C., & Beek, W. J. (2002). "Pumped-up propulsion" during front crawl swimming. *Medicine and Science in Sports and Exercise*, *34*, 314–319.